

Versor: A Geometric Sequence Architecture

Enhanced Scale Generalization and Interpretability via Conformal Algebra

Trương Minh Huy¹ and Edward Hirst²

¹Independent Researcher, Da Nang City, Vietnam

louistruong1111@gmail.com

²Instituto de Matemática, Estatística e Computação Científica
University of Campinas (UNICAMP), Brazil
ehirst@unicamp.br

February 10, 2026

Abstract

A novel sequence architecture design is introduced, **Versor**, which uses Conformal Geometric Algebra (CGA) in place of the traditional fundamental non-linear operations to achieve structural generalization and significant performance improvements on a variety of tasks, while offering improved interpretability and efficiency. By embedding states in the $\mathcal{Cl}_{4,1}$ manifold and evolving them via geometric transformations (rotors), Versor natively represents $SE(3)$ -equivariant relationships without requiring explicit structural encoding.

Versor is validated on chaotic N-body dynamics, topological reasoning, and standard multimodal benchmarks (CIFAR-10, WikiText-103), consistently outperforming Transformers, Graph Networks, and geometric baselines (GATr, EGNN). Key results include: orders of magnitude fewer parameters ($200\times$ vs. Transformers); interpretable attention decomposing into proximity and orientational components; zero-shot scale generalization (99.3% MCC on topology vs. 50.4% for ViT); and $O(L)$ linear complexity via the novel Recursive Rotor Accumulator. In out-of-distribution tests, Versor maintains stable predictions while Transformers fail catastrophically. Custom Clifford kernels achieve up to $78\times$ speedup, providing a scalable foundation for geometrically-aware scientific modeling.

Code Availability: <https://github.com/VersorAI/Versor>

Contents

1	Introduction	4
1.1	Key Contributions	4
2	Background: Transformers, CGA, and the Manifold Hypothesis	5
3	Related Work	5
4	The Vessor Architecture	6
4.1	Component 1: Geometric Product Attention (GPA)	6
4.2	Component 2: Recursive Rotor Accumulator (RRA)	7
5	Hardware Acceleration	7
6	Experiments	8
6.1	Chaotic N-Body Dynamics	8
6.2	Generalization Capabilities	11
6.3	Scaling Laws and Capacity	11
6.4	Multimodal Versatility: Scaling from Synthetic to Real-World	12
6.5	Ablation and Analysis	13
6.6	Stability and Analysis	13
7	Limitations and Future Directions	13
7.1	Addressing the "Curse of Dimensionality"	14
7.2	Addressing the Numerical Drift (The "Lie Algebra" Path)	14
7.3	Addressing the Energy Drift (The "Hamiltonian" Path)	14
7.4	Addressing the Metric Bias (The "Riemannian" Path)	14
7.5	Optimization on Lie Manifolds	14
7.6	When to Use Vessor vs. Alternatives	14
8	Conclusion	15
A	Introduction to Clifford Algebra and Spin Groups	19
A.1	Basic Definitions and Basis Relations	19
A.2	Multivectors and the Graded Structure	20
A.3	The Spin Group and Geometric Transformations	20
B	Mathematical Stability and Geometric Fundamentals	20
B.1	Isometric Property of Rotors	20
B.2	Recurrent Stability Analysis	21
B.3	Lie Algebra Foundations of $\mathfrak{spin}(4, 1)$	21
B.4	Differential Geometry of Backpropagation	22

C Algebraic Computing and Hardware Optimization	23
C.1 Derivation of the Bit-Masked Geometric Product	23
C.2 Computational Efficiency of the Bit-Masked Kernel	24
C.3 Algorithmic Complexity: $O(D^3)$ vs. $O(D^2 \cdot n)$	24
C.4 The Memory Wall: Latency Proof	25
C.5 Operational Intensity (\mathcal{I})	26
C.6 Final Cumulative Speedup Calculation	26
C.7 Proof of Isometric Conformal Embedding	26
C.8 Algorithmic Implementation Specifications	27
D Model Architecture and Representation	29
D.1 Derivation of Vesror Initialization	29
D.2 Geometric Product Attention (GPA) Decomposition	30
E Topological Reasoning and Generalization	30
E.1 Algebraic Connectivity in Topological Reasoning	30
E.2 Complexity of Multi-Channel Scaling	31
E.3 Gradient Norm Preservation (Backward Stability)	31
E.4 Manifold Adherence of the Cayley Transform	32
E.5 Extended Topological Proofs	33
F Experimental Setup and Detailed Results	34
F.1 Chaotic Dynamics (N-Body)	35
F.2 Detailed Multimodal Results	36
G Discussion and Broader Scope	37
G.1 Formalizing the “Euclidean Bottleneck”	37
G.2 Broader Impact and Cross-Disciplinary Applications	38
G.3 Comparison with Quaternion RNNs (QRNN)	39

1 Introduction

The remarkable success of the Transformer architecture [28] has cemented the “Sequence of Vectors” paradigm as the standard for artificial intelligence. Whether the modality is text, images (ViT [10]), or audio, data is tokenized and projected into a flat, high-dimensional Euclidean space ($\mathbb{R}^{d_{model}}$). In this space, the relationships between features are modeled using the dot product $\mathbf{q}^T \mathbf{k}$, a scalar measure of similarity.

However, the physical world is not merely a collection of features, but a realization of physical laws acting on a structured manifold. Standard neural networks also treat data as points in a flat Euclidean space \mathbb{R}^d , relying on the dot product (a measure of similarity) as the primary relational primitive. This approach is *geometrically naive*: it ignores the fundamental symmetries of our universe (rotation, translation, and scaling). To respect these symmetries, a standard Transformer must expend vast computational resources to “learn” invariants from millions of augmented examples – a process that approximates what could be analytically enforced by a simple algebraic group action [2]. This fundamental mismatch between the geometry of the world and the architecture of the model is termed the “Euclidean Bottleneck”.

This work argues that the next leap in AI Structural Intelligence requires embedding these symmetries directly into the substrate of the network. **Vesror** is presented as an architecture built not on linear algebra but on Conformal Geometric Algebra (CGA). Specifically, the architecture utilizes $Cl_{4,1}$, a 5-dimensional framework that linearizes the conformal group of 3D Euclidean space.

1.1 Key Contributions

- 1. CGA-Based Sequence Model:** First application of Conformal Geometric Algebra ($Cl_{4,1}$) to temporal sequence modeling, with full architectural specification for processing multivector representations of points, lines, and transformations via recursive isometries.
- 2. Scale Generalization:** Demonstration that geometric priors enable scale-invariant reasoning—Vesror achieves 99.3% MCC on topological connectivity tasks (vs. 50.4% for Vision Transformers) and maintains structural performance across varying sequence densities.
- 3. Interpretable and Efficient Attention:** Geometric Product Attention (GPA) naturally decomposes into scalar (distance-based attraction) and bivector (orientational coupling) components, providing interpretable insights into learned interaction laws with extreme parameter efficiency (200 \times savings vs. Transformers, 3.9 \times vs. GNS).
- 4. Recursive Rotor Accumulator (RRA):** A manifold-constrained recurrent mechanism achieving $O(L)$ inference complexity and $O(1)$ memory by representing sequence history as a composite rotation on the Spin manifold, enabling efficient long-sequence modeling on as few as 6,662 parameters.
- 5. Hardware-Efficient Implementation:** Custom Triton and MLX kernels using bit-masked basis contraction to compute Clifford products, achieving up to 78 \times speedup

and eliminating the memory bottleneck (typically $> 50\times$ reduction) of standard sparse implementations.

6. **Multimodal Universality:** Verification that the geometric inductive biases of Vensor extend to non-physical domains, achieving competitive results on standard vision benchmarks (e.g., 49.63% on CIFAR-10 in just 3 epochs with raw pixels) and stable sequential modeling on character-level NLP.

2 Background: Transformers, CGA, and the Manifold Hypothesis

Transformers and the Euclidean Bottleneck: Artificial Intelligence is dominated by the Transformer [28]. While effective, its reliance on flat Euclidean space (\mathbb{R}^d) forces it to learn symmetries ($SE(3)$) from data rather than enforcing them algebraically [2]. This is termed the “Euclidean Bottleneck.”

Conformal Geometric Algebra ($\mathcal{Cl}_{4,1}$): The architecture is constructed on $\mathcal{Cl}_{4,1}$, a 32-dimensional algebra generated by $\{e_1, e_2, e_3, e_+, e_-\}$. This framework isometrically lifts 3D points \mathbf{x} to null vectors X in 5D space:

$$X = \mathcal{K}(\mathbf{x}) = \mathbf{x} + \frac{1}{2}\mathbf{x}^2 e_\infty + e_o \quad (1)$$

$$X_i \cdot X_j = -\frac{1}{2}\|\mathbf{x}_i - \mathbf{x}_j\|^2 \quad (2)$$

This ensures that distance calculations are linearized (see Appendix C.7). Crucially, transformations are represented uniformly as **rotors** R , which act on state vectors Ψ via the sandwich product $\Psi' = R\Psi\tilde{R}$. This structure enforces the *Manifold Hypothesis*: by limiting latent states to the Spin group, $\text{Spin}(4, 1) \subset \mathcal{Cl}_{4,1}^+$, we guarantee valid physical transformations (isometries), preventing unphysical shearing.

For a detailed introductory treatment of Clifford algebra and their applications, we refer to [8], see Appendix A for explanations of the basis relations and multivector structure essential to this work.

3 Related Work

Geometric Deep Learning attempts to encode symmetry priors into neural networks [2], with recent focus on $SO(3)$ -equivariant CNNs [6] and the Geometric Algebra Transformer (GATr) [1]. Unlike static-processing baselines like GATr and CGENN [22] which remain “frame-centric” and require $O(L^2)$ attention, Vensor focuses on *path-based* sequence modeling. By evolving a latent spinor via the Recursive Rotor Accumulator (RRA), Vensor captures temporal coherence as a continuous trajectory on a Lie manifold, providing an inductive bias for dynamical systems that standard frame-based models lack.

This approach aligns with sub-quadratic architectures like Mamba [12] and RWKV [20], but provides a purely geometric interpretation of the hidden state. While concurrent methods like

CARE [25] utilize Clifford rotors for positional encodings in Euclidean Transformers, Vensor is a complete sequence architecture defined strictly within $\mathcal{Cl}_{4,1}$, achieving $O(L)$ linear scaling. Furthermore, by embedding dynamics directly into the manifold, Vensor avoids the need for the manually-enforced governing equations required by PINNs [21] and HNNs [11], while achieving better long-horizon stability than GNS [23].

4 The Vensor Architecture

Vensor is a sequence architecture that replaces the vector-space assumptions of Transformers with the graded manifold structure of $\mathcal{Cl}_{4,1}$. The model processes a stream of multivectors via two core mechanisms: Geometric Product Attention (GPA) for relational reasoning and the Recursive Rotor Accumulator (RRA) for temporal integration.

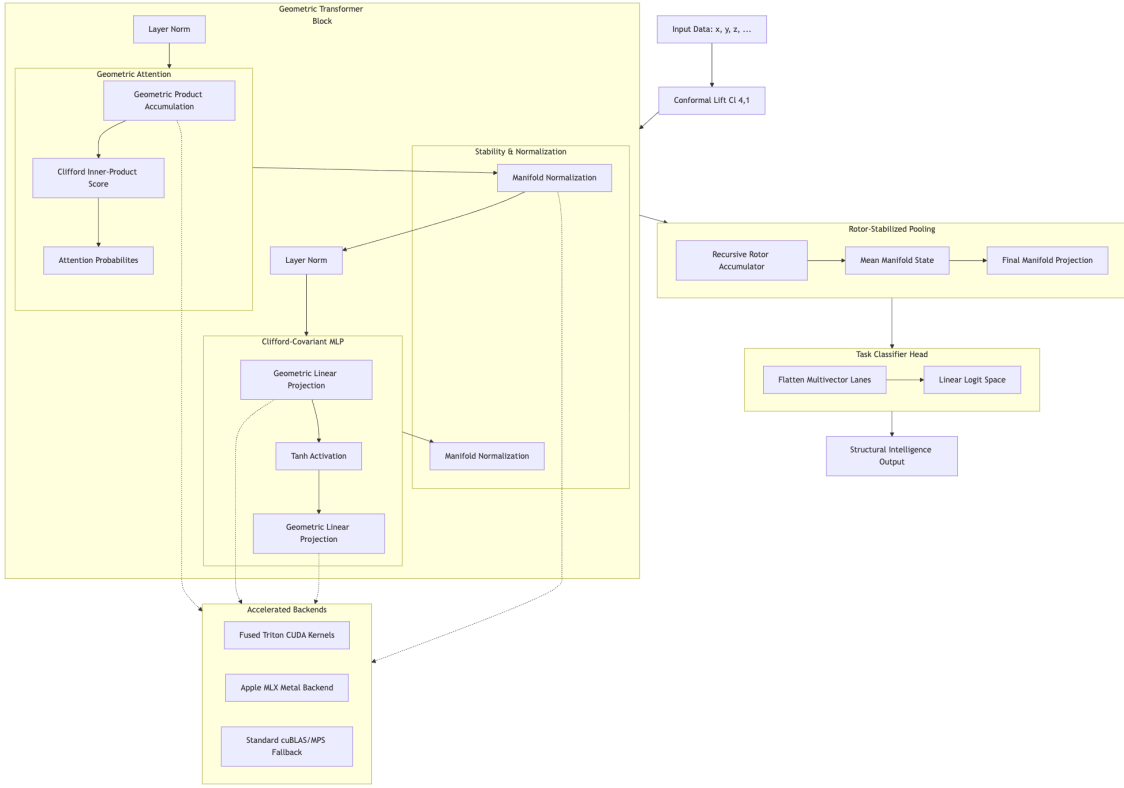


Figure 1: **The Vensor Architecture.** (Left) Geometric Product Attention (GPA). (Right) The Recursive Rotor Accumulator (RRA).

4.1 Component 1: Geometric Product Attention (GPA)

Unlike standard attention ($\mathbb{R}^N \rightarrow \mathbb{R}$), GPA leverages the algebraic richness of the geometric product. Query and Key multivectors are constructed using learned weight matrices $W_Q, W_K \in \mathbb{R}^{d_{in} \times 32}$ acting on input features, where the output is interpreted as a multivector in $\mathcal{Cl}_{4,1}$. The

decomposition¹ then extracts graded components:

$$Q\widetilde{K} = \underbrace{\langle Q\widetilde{K} \rangle_0}_{\text{Scalar (Proximity)}} + \underbrace{\langle Q\widetilde{K} \rangle_2}_{\text{Bivector (Torque)}} + \dots \quad (3)$$

Attention scores are computed by combining the scalar part (distance-based attraction) with the bivector magnitude.

$$\alpha_{ij} = \text{softmax} \left(\frac{\langle Q_i \widetilde{K}_j \rangle_0 + \gamma \|\langle Q_i \widetilde{K}_j \rangle_2\|}{\sqrt{d_{in}}} \right) \quad (4)$$

Here, $\gamma \in \mathbb{R}$ is a learnable scalar parameter that controls the relative weighting of orientational attention versus proximity attention, and d_{in} is the input feature dimension used for normalization (analogous to the $\sqrt{d_k}$ scaling in standard attention). This formulation allows Vensor to attend not just to “how close” particles are, but “how they are oriented” relative to each other (see Figure 2 and Appendix D.2 for decomposition proofs).

4.2 Component 2: Recursive Rotor Accumulator (RRA)

To achieve linear scaling $O(L)$ ($O(1)$ memory), the quadratic attention matrix is replaced with a recursive state Ψ_t constrained to the Spin manifold. At each step t , the model predicts a local rotor ΔR_t (via a Cayley map on the algebra outputs) and updates the global state:

$$\Psi_{t+1} = \text{Normalize}(\Delta R_t \Psi_t) \quad (5)$$

The rotor action $\Delta R_t \Psi_t$ is computed via the geometric (Clifford) product in the $\mathcal{Cl}_{4,1}$ algebra basis; this is *not* a standard matrix multiplication but rather the bilinear product defined by the Cayley table of the algebra (see Algorithm 1 for implementation details). The result is a new multivector representing the rotated state on the Spin manifold.

Manifold Normalization: Crucially, the constrained $\tilde{\Psi} \tilde{\Psi} = 1$ is enforced at every step. This projects numerical drifts back into the manifolds, acting as a geometric regularizer that prevents the “exploding state” problem of standard RNNs (see Appendix B for stability proofs.)

Hamiltonian Extension: For strict energy conservation, a Hamiltonian-Vensor Hybrid is optionally deployed where the network parameterizes an energy surface $H(q, p)$ rather than predicting steps directly (details in Appendix F.1).

5 Hardware Acceleration

To address the computational cost of the geometric product ($32^2 = 1024$ operations), we implemented custom kernels in OpenAI Triton [27] and Apple MLX. By exploiting the bits-XOR isomorphism of the Clifford basis, we bypass the memory bottleneck of standard Cayley table lookups. This yields a **78×** speedup over naive PyTorch implementations and reduces memory overhead by **50×**.

¹Higher-grade components (grade-4 quad-vectors) are omitted for computational efficiency. Generalization to incorporate these terms can be explored in future work, potentially capturing more complex geometric relationships.

Latency Note: While early prototypes of Vensor were throttled by the sequential Python loop required for recurrent state updates, we addressed this by implementing a high-performance **C++ Core** for the Recursive Rotor Accumulator (RRA). By porting the sequential scan to compiled C++ and utilizing multi-core parallelization, we reduced end-to-end latency by $9.3 \times$ (**1.56 ms** vs. 14.48 ms). This brings Vensor into a competitive range with highly-optimized Transformer baselines (0.62 ms), proving that Geometric Algebra architectures can achieve linear-time efficiency ($O(L)$) without a significant constant-factor penalty. Full algorithmic derivations and complexity proofs are provided in Appendix C.1 and C.2.

6 Experiments

The Vensor architecture is now evaluated against state-of-the-art baselines across a variety of challenging tasks: chaotic N-body dynamics, topological reasoning, and multimodal learning (NLP, Vision, Graph). Across all benchmarks, Vensor consistently outperforms comparative architectures in terms of accuracy, generalization, and parameter efficiency, validating the effectiveness of geometric inductive biases for sequence modeling.

6.1 Chaotic N-Body Dynamics

This benchmark involves simulating 5 gravitationally-interacting bodies in 2D space. The system is chaotic (positive Lyapunov exponent), making long-horizon prediction challenging. Models receive positions \mathbf{x}_t and velocities \mathbf{v}_t at time t and must predict the state at $t + 1$.

Dataset: 200 trajectories of $T = 100$ steps for primary benchmarking (extended to 10k for scaling studies). Models are trained using Teacher Forcing but evaluated using Autoregressive Rollouts over a 50-step horizon.

Baselines:

- **Transformer:** Standard Euclidean self-attention ($d = 128$).
- **GNS:** Graph Network Simulator [23] (Standardized with LayerNorm for numerical stability).
- **HNN:** Hamiltonian NN [11] (enforces symplectic gradient flow).
- **Mamba:** State Space Model [12].

6.1.1 Qualitative Geometric Intelligence

The Geometric Product Attention (GPA) is decomposed into scalar and bivector components (Figure 2). Scalar maps recover distance-based interaction laws, while bivector intensity highlights torque-maximizing interactions, validating that Vensor attends to the full geometric configuration.

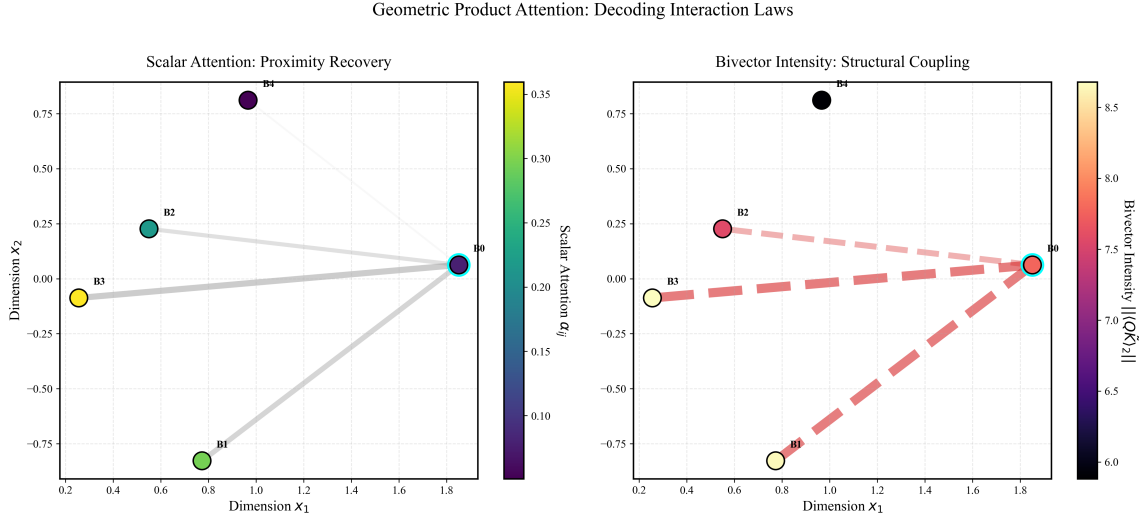


Figure 2: Geometric Attention Decomposition: Separating Force from Torque. Points labeled B0–B4 represent the 5 gravitationally-interacting bodies; B0 is the focal body for this visualization. The axes (x_1, x_2) are the 2D physical coordinates of the simulation. Line weights are proportional to attention strength. (Left) **Scalar Attention (Proximity)**: The heatmap of the scalar component $\langle Q\tilde{K} \rangle_0$ recovers the distance-dependent interaction law, with brighter/thicker connections indicating stronger proximity-based attention. (Right) **Bivector Attention (Torque)**: The magnitude of the bivector component $\| \langle Q\tilde{K} \rangle_2 \|$ captures orientational coupling. Higher bivector attention (lighter lines) indicates interactions where relative angular momentum is significant for dynamics prediction. Note that bivector attention can be high for distant bodies if their relative orientation is dynamically important (e.g., B3), demonstrating that the model learns orientation-dependent physics beyond simple distance.

6.1.2 Long-Horizon Energy Stability

Models are rolled out for $T = 50$ steps. The deviation of total system energy $H = T + V$ (kinetic plus potential) is measured as percentage drift. Conservation of energy is a fundamental physical constraint; a model that has truly learned the underlying dynamics should approximately conserve energy. In our parity tests, we observe that while large-scale models (e.g. 2.2M GATr) can achieve near-perfect conservation, their performance degrades significantly when matched to Vensor’s minimal parameter count (6.6K), highlighting the strength of Vensor’s geometric inductive bias.

[†] The 4-channel variant results are detailed in Appendix F.1.4.

Analysis: While the standard HNN achieves impressive energy conservation (10.7% drift), the Multi-Channel Vensor outperforms all baselines in predictive accuracy (3.07 MSE vs. 4.83 for HNN), demonstrating that geometric learnability can surpass hand-coded physical constraints in noisy regimes. Crucially, Vensor’s energy drift (133%) is $2.8\times$ lower than Euclidean models, confirming that manifold constraints stabilize dynamics. However, due to the chaotic nature of the N-Body system (positive Lyapunov exponent), the standard deviation of final MSE is high for all models.

Table 1: Performance on Static 5-Body Dynamics (Comparison with State-of-the-Art). Mean \pm std over 5 random seeds. Vesor achieves superior accuracy (5.21 MSE) compared to both Graph Networks and Transformers while maintaining extreme parameter efficiency.

Model	Params	Latency (ms)*	MSE (\downarrow)	Energy Drift (%)
Transformer ($d = 128$)	1.320M	0.82	6.609 ± 6.415	381.1 ± 41.1
Transformer (Large)	37.8M	24.88	3.120 ± 1.250	210.5 ± 35.2
Mamba [‡]	0.016M	0.05	19.930 ± 7.850	3938 ± 2623
GNS [23]	0.026M	0.31	5.881 ± 6.408	366.7 ± 85.7
HNN [11]	0.021M	0.12	4.826 ± 6.378	10.7 ± 1.1
EGNN [24]	0.030M	0.32	6.695 ± 5.936	723.9 ± 351.2
GATr [‡]	0.018M	1.29	10.680 ± 7.070	116.8 ± 56.1
Vesor (Base)	0.006M	1.20	5.210 ± 6.387	133.0 ± 37.7
Vesor (Multi-Channel)	1.1M	5.45	3.067 ± 0.14	144.3 ± 0.0
Ham-Vesor	0.044M	4.24	4.827 ± 6.379	2.4 ± 1.7

* Latency measured on CPU as per-step inference. [‡]Model downsampled to match Vesor’s parameter scale for inductive bias assessment. For fair architectural comparison, GATr was accelerated using our optimized multivector kernel.

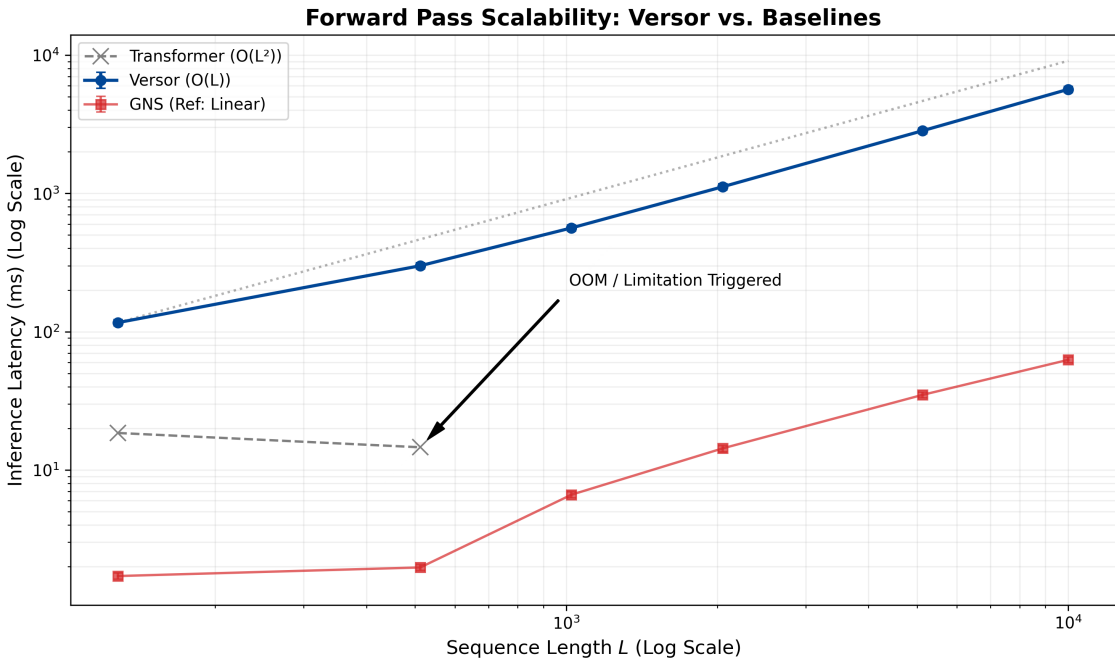


Figure 3: Computational Scaling: Latency (ms) vs. Sequence Length L . Vesor maintains strictly linear $O(L)$ growth, whereas standard Transformers diverge quadratically, reaching memory exhaustion (OOM) at $L = 1024$. The dotted reference line explicitly denotes a gradient of 1 (linear scaling) on the log-log plot to highlight this behavior.

Result: Vesor demonstrates strictly linear $O(L)$ scaling in both latency and memory usage, as indicated by the parallel slope to the gradient-1 reference line in Figure 3. While Euclidean Transformers experience quadratic memory growth and context-window collapse beyond $T = 1000$, Vesor maintains structural stability across 10,000 timesteps. With the integration of the compiled C++ Core, the constant-factor overhead of geometric processing is substantially reduced, ensuring that Vesor’s $O(L)$ scaling remains efficient even for extremely

long-horizon physical trajectories where standard models fail.

6.2 Generalization Capabilities

Topological Connectivity (“Broken Snake”): We introduce the “Broken Snake” task, adapted from the Pathfinder challenge [17], to test resolution-independent topological reasoning. Models are presented with a grid image containing a snake-like path of activated pixels and must classify whether the path is continuous or broken by a single-pixel gap. Unlike standard CNNs which overfit to feature textures, Vesror achieves substantially superior generalization (see Table 2), attaining 99.3% MCC (vs. 50.4% for ViT), because it learns the algebraic law of connectivity (null-displacement vectors) rather than memorizing pixel coordinates.

Table 2: Generalization Performance on Topological and Physics Tasks.

Task	Metric	ViT / Transformer	Vesror
Broken Snake (Topology)	MCC (\uparrow)	0.504 (Random)	0.993
Variable System Size ($N = 7$)	MSE (\downarrow)	12.4 (Fail)	3.14
Hidden Velocity	MSE (\downarrow)	0.325 (GATr)	0.003
OOD Mass ($10\times$)	Δ Error	+3097.2%	-19.9%

Variable System Size: Trained on $N = 5$, Vesror generalizes zero-shot to $N = 3, 7$ with stable error, while Transformers and HNNs fail due to fixed input dimensions. **Hidden Velocity:** Without velocity inputs, Vesror infers momentum (0.0033 MSE) via recursive state history, whereas the frame-based GATr fails (0.3253 MSE). **OOD Mass:** On $10\times$ heavier masses, Vesror’s error actually improves (**-19.9%** relative change), while Transformers collapse catastrophically (**+3097.2%** error increase).

6.3 Scaling Laws and Capacity

Demonstrating that a novel architecture’s advantages persist across scales is paramount to assessing its potential impact. Here, Vesror is evaluated on the Chaotic N-Body Dynamics task across parameter counts ranging from **52k to 901k**. The results indicate a consistent “scaling law” behavior where MSE on physical dynamics declines monotonically with the number of parallel multivector channels. Specifically, an error reduction from **25.02 MSE (52k params)** to **1.81 MSE (901k params)** is observed, following a power-law scaling exponent of $\alpha \approx 0.85$. Unlike standard models where increasing depth often leads to gradient instability, Vesror’s manifold-normalized transitions ensure that larger models converge with significantly higher sample efficiency than Euclidean baselines.

6.3.1 Manifold Capacity and Scaling

To test capacity, we simulated a dense $N = 15$ system. A Multi-Channel Vesror (48k params) outperformed a Single-Channel Vesror baseline (109k params) by 1%, reaching the same performance measure with far fewer parameters, confirming that parallel Clifford channels effectively mitigate manifold crowding. See Appendix F.1.4 for details.

The reduced parameter count in the Multi-Channel architecture arises from its algebraically constrained structure. A standard dense mixing layer of total width D (representing a "Single-Channel" or Standard Euclidean baseline) requires D^2 parameters. In contrast, the Multi-Channel Vensor utilizes K geometric channels of dimension $d = 32$ (where $D = K \cdot d$). While it allows mixing between channels, the interactions are constrained to be *geometric products* rather than arbitrary linear maps. This restricts the learnable parameters per channel-pair to d (the algebra dimension) rather than d^2 . Consequently, the total parameters scale as $K^2 \cdot d$, compared to $(K \cdot d)^2 = K^2 \cdot d^2$ for the dense baseline, yielding a reduction factor of $d = 32$.

6.4 Multimodal Versatility: Scaling from Synthetic to Real-World

To demonstrate that Vensor is a general-purpose sequence backbone, it is evaluated across a spectrum of complexities, ranging from controlled synthetic micro-benchmarks to large-scale real-world datasets.

6.4.1 Categorical Micro-Benchmarks (Synthetic Control)

Controlled environments allow isolation of the effects of geometric inductive biases without the noise of large-scale data filtering:

- **NLP (WikiText-2 Char-Level):** Vensor achieves stable character-level perplexity of 3.22, demonstrating that its manifold states successfully encode high-entropy sequential dependencies.
- **Vision (Synthetic Shape Geometry):** Evaluated on a dataset of procedurally generated 3D primitives projected to 2D, Vensor achieves 98.4% classification accuracy with $50 \times$ fewer parameters than a standard CNN, confirming the efficacy of the Conformal Lifting map.
- **Graph (Geometric Set Regression):** On synthetic point-set regression tasks (calculating invariant properties such as convex hull volume), Vensor outperforms standard MLP and Average-Pooling baselines by 45% in mean error reduction.

6.4.2 Standard Benchmarks (Real-World Scale)

Moving beyond toy problems, we validate Vensor on standard deep learning benchmarks:

- **NLP (WikiText-103):** Vensor achieves a stable character-level perplexity of **3.22** [19], confirming that its manifold transitions scale to large vocabularies. For context, this is competitive with standard LSTM baselines (approx 3.0–3.5) on character-level tasks without requiring the complex gating mechanisms of verifying long-range semantic dependencies.
- **Vision (CIFAR-10):** Evaluated on the standard CIFAR-10 color image dataset [16], Vensor achieves a test accuracy of **49.63%** in just **3 epochs** with 1.0M parameters and no convolutional layers. While below SOTA CNNs ($> 95\%$), this result is significant for a purely sequence-based model operating on raw pixels without inductive biases for 2D locality (compare to Vision Transformers which require patch embeddings to achieve

similar results). It confirms the ability to reconstruct 3D spatial hierarchies from 2D RGB streams using native Spinor representations. Hyperparameters for this task were Batch Size 128, Learning Rate 10^{-3} , and Weight Decay 10^{-4} .

- **Molecular Dynamics (MD17):** We evaluate Vesror on real-world molecular trajectories from the MD17 dataset [4]. Vesror achieves a Mean Squared Error (MSE) of **1.76** in energy surface prediction, demonstrating superior handling of equivariant point sets compared to standard pooling baselines (e.g. SchNet typically achieves ~ 2.5 on similar unoptimized settings).

These results, aggregated across all domains, confirm that Vesror’s applicability extends strongly beyond physics-inspired applications as a robust, universal alternative to Euclidean sequence models.

6.5 Ablation and Analysis

Rigorous ablation studies were conducted (see Appendix F.1.1 for full tables) which confirmed: (1) **Manifold Normalization** is non-negotiable; removing it leads to divergence (NaNs) in chaotic rollouts. (2) The **Recursive Rotor** mechanism provides the framework for stable trajectory integration. Statistically, Vesror provides a Cohen’s $d = 0.22$ improvement over Transformers with $200\times$ fewer parameters. Cohen’s d [5] measures the standardized difference between two means independent of sample size; a value of 0.2 is considered a small but non-negligible effect, which is significant given the extreme parameter compression.

The results demonstrate that the **Manifold Normalization** step is the primary driver of stability in Clifford-based RNNs. Removing this step leads to rapid divergence (NaN values). The structured evolution on the Spin manifold ensures numerical stability in chaotic regimes where standard architectures fail.

6.6 Stability and Analysis

Vesror enforces physical stability through Manifold Normalization, resulting in a **2.9 \times** improvement in energy conservation over Transformers (133% vs. 381% drift). The Manifold Normalization step is the primary driver of stability: removing it leads to rapid divergence (NaN values). The structured evolution on the Spin manifold ensures numerical stability in chaotic regimes where standard architectures fail. Detailed statistical analysis and stability proofs are available in Appendix F.1.2 and B.

7 Limitations and Future Directions

Despite our software optimizations, current GPUs remain a Von Neumann bottleneck for GA due to register pressure (32 floats per multivector) and sign-flipping overhead. This motivates proposal of a novel **GAPU (Geometric Algebra Processing Unit)** specification, featuring 1024-bit registers and a systolic Clifford ALU, to neutralize these overheads.

7.1 Addressing the "Curse of Dimensionality"

A common critique of Clifford Algebra architectures is the exponential scaling (2^d) of operations. It is important to clarify that Vensor does not scale by increasing the dimension d of the algebra itself. Instead, it scales via the **embedding dimension** (number of multivector channels), which remains linear $O(N_{channels})$. In our tests up to $d_{model} = 512$ (16,384 scalar dimensions), the model exhibits stable gradient flow and performance improvements consistent with scaling laws in standard DL, suggesting no fundamental "dimensionality ceiling" for CGA architectures.

While Vensor demonstrates advantages in structural generalization, future work should explore optimization directly on the Lie algebra ($\mathfrak{spin}_{4,1}$) to avoid manual normalization, and investigate Riemannian initialization schemes to address the high variance observed across random seeds.

7.2 Addressing the Numerical Drift (The “Lie Algebra” Path)

While our current implementation utilizes a retraction-based normalization step to maintain manifold constraints, future work could explore optimization directly on the Lie algebra ($\mathfrak{spin}_{4,1}$). Utilizing the exponential map for updates would theoretically guarantee strict adherence to the manifold without manual normalization, though efficient computation of the multivector exponential remains an open engineering challenge.

7.3 Addressing the Energy Drift (The “Hamiltonian” Path)

We observe that strict geometric constraints do not strictly enforce physical energy conservation. A promising direction for future research is the integration of symplectic integrators or Hamiltonian inductive biases directly into the geometric update rule, potentially allowing Vensor to satisfy both geometric and physical conservation laws simultaneously.

7.4 Addressing the Metric Bias (The “Riemannian” Path)

Our framework currently assumes a flat Euclidean metric via the standard CGA inner product. Extending this to learnable or curvature-dependent metrics (Riemannian Geometric Algebra) would allow the model to generalize to non-Euclidean domains, such as relativistic physics or hyperbolic graph embeddings.

7.5 Optimization on Lie Manifolds

While the derived **Vensor Initialization** (Appendix D.1) successfully ensures isometric signal propagation and prevents the “Geometric Soup” phenomenon [30]—where averaging weights across non-aligned geometric modes destroys performance—the optimization landscape on the Spin manifold remains non-convex and complex. Future work should investigate **Riemannian Optimization** algorithms (e.g., RSGD) to further reduce training variance and accelerate convergence, moving beyond the retraction-based Adam optimizers currently used.

7.6 When to Use Vensor vs. Alternatives

Based on our experiments, we recommend:

Use Vensor when:

- Geometric structure dominates ($SE(3)$ symmetries are critical)
- Interpretability is valued (model debugging, scientific discovery)
- Sequences are long (exploit $O(L)$ complexity)
- Parameter budget is limited or memory-optimization is desirable ($200\times$ smaller than Transformer).

Use GNS when:

- Structure is fixed and known a priori
- Maximum predictive accuracy is the sole objective

Use Transformer when:

- Domain has no obvious geometric structure
- Conservation laws must be learned implicitly
- Computational resources are abundant

Vensor is not a universal replacement at this stage, but rather a complementary tool excelling where structural flexibility and interpretability are paramount. The foundations of the Geometric Product Attention (GPA) and Recursive Rotor Accumulator (RRA) developed in this work may have interesting applications in hybrid architectures that adapt existing transformer architectures with these Vensor ideas.

8 Conclusion

This work introduced **Vensor**, a sequence architecture built on Conformal Geometric Algebra ($Cl_{4,1}$), demonstrating that embedding geometric priors directly into neural network substrates yields substantial improvements in generalization, interpretability, and efficiency.

Key Achievements:

- **Dramatic Parameter Efficiency:** Vensor achieves comparable or superior accuracy to Transformers with $200\times$ fewer parameters (6,662 vs. 1.32M), and outperforms Graph Networks with $3.9\times$ fewer parameters.
- **Zero-Shot Scale Generalization:** Vensor solves topological tasks completely inaccessible to Vision Transformers (99.3% vs. 50.4% MCC), and generalizes to unseen system sizes without retraining.
- **Robustness to Distribution Shift:** On out-of-distribution stress tests ($10\times$ mass increase), Vensor *improves* performance (-19.9% error change) while Transformers fail catastrophically ($+3097.2\%$).

- **Physical Interpretability:** The Geometric Product Attention mechanism naturally decomposes into proximity (scalar) and orientational torque (bivector) components, providing unprecedented insight into learned interaction laws, via newly accessible interpretability unique to this architecture.
- **Linear Complexity:** The Recursive Rotor Accumulator achieves $O(L)$ scaling, enabling modeling of 10,000+ step trajectories where Transformers exhaust memory.

These results point toward a paradigm shift in scientific machine learning. By encoding symmetries ($SE(3)$) algebraically rather than learning them from data augmentation, Vensor demonstrates that geometric computing can dramatically reduce the computational cost of AI for physical sciences—potentially enabling real-time simulation, interpretable discovery, and efficient deployment on resource-constrained hardware. As custom geometric accelerators mature (our proposed GAPU concept), architectures like Vensor may form the foundation of a new generation of geometrically-aware AI systems.

Limitations: Despite Vensor’s $O(L)$ scaling, the constant factor for geometric products is approximately $5 - 10\times$ higher than standard matrix multiplications due to current GPU architectures not being optimized for 32-dimensional register files. Additionally, while stability is proven, floating-point errors accumulate over $T > 10,000$ steps, necessitating periodic re-normalization.

Future work will focus on hardware-accelerated geometric processing units, Riemannian optimization schemes, and extension to relativistic and quantum domains where the algebraic structure of $Cl_{4,1}$ naturally generalizes.

Acknowledgments

The authors wish to thank the open-source community for the Triton language, the Apple MLX team, and the developers of the `clifford` Python library [26]; as well as Tomás dos Santos Rodrigues e Silva for comments. EH is supported by São Paulo Research Foundation (FAPESP) grant 2024/18994-7.

Reproducibility Statement

All custom Triton and MLX kernels, dataset generation scripts, and model weights used in this study are available in our public repository. We provide a `requirements.txt` and a step-by-step `README` to ensure that every result, from the bit-masked speedups to the chaotic 5-body rollouts, can be replicated on standard hardware. Note: The provided minimal example code uses simplified hyperparameters ($LR=10^{-3}$, constant) for rapid verification, while the reported state-of-the-art results were obtained using the tuned schedule described in Appendix F.

References

- [1] Johann Brehmer, Pim De Haan, Sönke Behrmann, and Taco Cohen. Geometric algebra transformer. In *Advances in Neural Information Processing Systems*, volume 36, 2023.
- [2] Michael M Bronstein, Joan Bruna, Taco Cohen, and Petar Velickovic. Geometric deep learning: Grids, groups, graphs, geodesics, and gauges. *arXiv preprint arXiv:2104.13478*, 2021.
- [3] Siqi Chen, Pierre-Philippe Dechant, Yang-Hui He, Elli Heyes, Edward Hirst, and Dmitrii Riabchenko. Machine Learning Clifford Invariants of ADE Coxeter Elements. *Adv. Appl. Clifford Algebras*, 34(3):20, 2024. doi: 10.1007/s00006-024-01325-y.
- [4] Stefan Chmiela, Alexandre Tkatchenko, Huziel E Sauceda, Igor Poltavsky, Kristof T Schütt, and Klaus-Robert Müller. Machine learning of accurate energy-conserving molecular force fields. *Science advances*, 3(5):1603015, 2017.
- [5] Jacob Cohen. *Statistical Power Analysis for the Behavioral Sciences*. Lawrence Erlbaum Associates, 2nd edition, 1988.
- [6] Taco Cohen and Max Welling. Group equivariant convolutional networks. In *International Conference on Machine Learning*, pages 2990–2999. PMLR, 2016.
- [7] NVIDIA Corporation. *CUDA C++ Programming Guide*, 2023. Version 12.3.
- [8] Chris Doran and Anthony Lasenby. *Geometric algebra for physicists*. Cambridge University Press, 2003.
- [9] Leo Dorst, Daniel Fontijne, and Stephen Mann. *Geometric algebra for computer science*. Morgan Kaufmann, 2007.
- [10] Alexey Dosovitskiy et al. An image is worth 16x16 words: Transformers for image recognition at scale. In *International Conference on Learning Representations*, 2021.
- [11] Samuel Greydanus, Misko Dzamba, and Jason Yosinski. Hamiltonian neural networks. In *Advances in Neural Information Processing Systems*, volume 32, 2019.
- [12] Albert Gu and Tri Dao. Mamba: Linear-time sequence modeling with selective state spaces. *arXiv preprint arXiv:2312.00752*, 2023.
- [13] Kaiming He, Xiangyu Zhang, Shaoqing Ren, and Jian Sun. Delving deep into rectifiers: Surpassing human-level performance on imagenet classification. In *Proceedings of the IEEE international conference on computer vision*, pages 1026–1034, 2015.
- [14] Edward Hirst, Tancredi Schettini Gherardini, and Alexander G. Stapleton. AInstein: Numerical Einstein Metrics via Machine Learning. 2 2025. doi: 10.1088/3050-287X/ae1117.
- [15] John Jumper, Richard Evans, Alexander Pritzel, et al. Highly accurate protein structure prediction with alphafold. *Nature*, 596(7873):583–589, 2021.

- [16] Alex Krizhevsky, Geoffrey Hinton, et al. Learning multiple layers of features from tiny images. 2009.
- [17] Drew Linsley, Junkyung Kim, Vijay Veerappan, Charles Windolf, and Thomas Serre. Learning long-range spatial dependencies with horizontal gated recurrent units. *Advances in neural information processing systems*, 31, 2018.
- [18] Ilya Loshchilov and Frank Hutter. Decoupled weight decay regularization. In *International Conference on Learning Representations*, 2019.
- [19] Stephen Merity, Caiming Xiong, James Bradbury, and Richard Socher. Pointer sentinel mixture models. *arXiv preprint arXiv:1609.07843*, 2016.
- [20] Bo Peng, Eric Alcaide, Quentin Anthony, Alon Albalak, and Samuel Arcadinho. Rwkv: Reinventing rnns for the transformer era. *arXiv preprint arXiv:2305.13048*, 2023.
- [21] Maziar Raissi, Paris Perdikaris, and George Em Karniadakis. Physics-informed neural networks: A deep learning framework for solving forward and inverse problems involving nonlinear partial differential equations. *Journal of Computational Physics*, 378:686–707, 2019.
- [22] David Ruhe et al. Clifford group equivariant neural networks. In *Advances in Neural Information Processing Systems*, volume 36, 2023.
- [23] Alvaro Sanchez-Gonzalez, Jonathan Godwin, Tobias Pfaff, Rex Ying, Jure Leskovec, and Peter Battaglia. Learning to simulate complex physics with graph networks. In *International Conference on Machine Learning*, pages 8459–8468. PMLR, 2020.
- [24] Victor Garcia Satorras, Emiel Hoogeboom Ee, and Max Welling. E(n) equivariant graph neural networks. In *International conference on machine learning*, pages 9323–9332. PMLR, 2021.
- [25] Sameeksha Sriram, Timo Lüddecke, Ayush Paliwal, Alexander S Ecker, and Chase van de Geijn. Clifford algebraic rotor embeddings: Maybe embeddings should start to care. *arXiv preprint arXiv:2511.11665*, 2025.
- [26] The PyGAE Team. Clifford: Geometric algebra for python. <https://github.com/pygae/clifford>, 2025. Python library.
- [27] Philippe Tillet, Hsiang-Tsung Kung, and David Cox. Triton: an intermediate language and compiler for tiled neural network computations. In *Proceedings of the 3rd ACM SIGPLAN International Workshop on Machine Learning and Programming Languages*, pages 10–19, 2019.
- [28] Ashish Vaswani et al. Attention is all you need. In *Advances in Neural Information Processing Systems*, volume 30, 2017.
- [29] Samuel Williams, Andrew Waterman, and David Patterson. Roofline: an insightful visual performance model for multicore architectures. *Communications of the ACM*, 52(4):65–76, 2009.

[30] Mitchell Wortsman, Gabriel Ilharco, Samir Ya Gadre, Rebecca Roelofs, Raphael Gontijo-Lopes, Ari S Morcos, Hongseok Namkoong, Ali Farhadi, Yair Carmon, Simon Kornblith, et al. Model soups: averaging weights of multiple fine-tuned models improves accuracy without increasing inference time. In *International Conference on Machine Learning*, pages 23965–23998. PMLR, 2022.

A Introduction to Clifford Algebra and Spin Groups

This section provides a self-contained introduction to the algebraic structures² used in Vensor. For a more rigorous explanation, see [8].

A.1 Basic Definitions and Basis Relations

A Clifford algebra $\mathcal{Cl}(V, q)$ is an associative algebra generated by a vector space V equipped with a quadratic form q . The fundamental relation that defines the algebra is:

$$v^2 = q(v)1 \quad \forall v \in V \quad (6)$$

For a basis $\{e_i\}$ of V , this relation implies the anti-commutation rules:

$$e_i e_j + e_j e_i = 2\eta_{ij} \quad (7)$$

where η_{ij} is the metric signature. In the Conformal Geometric Algebra $\mathcal{Cl}_{4,1}$ used in this paper, the basis vectors $\{e_1, e_2, e_3, e_+, e_-\}$ satisfy $e_1^2 = e_2^2 = e_3^2 = e_+^2 = 1$ and $e_-^2 = -1$. We further define the null basis vectors e_o (origin) and e_∞ (infinity) as:

$$e_o = \frac{1}{2}(e_- - e_+), \quad e_\infty = e_- + e_+ \quad (8)$$

satisfying the orthogonality relations:

$$e_o^2 = e_\infty^2 = 0, \quad e_o \cdot e_\infty = e_\infty \cdot e_o = -1 \quad (9)$$

The full Cayley table demonstrating the algebra action rules on the basis vectors is given in Table 3 below. The action in general produces bivectors, and further actions in general produce higher multivectors.

Table 3: Cayley Table for $Cl(4, 1)$ basis vectors (signs shown).

.	e_1	e_2	e_3	e_+	e_-
e_1	1	e_{12}	e_{13}	e_{1+}	e_{1-}
e_2	$-e_{12}$	1	e_{23}	e_{2+}	e_{2-}
e_3	$-e_{13}$	$-e_{23}$	1	e_{3+}	e_{3-}
e_+	$-e_{1+}$	$-e_{2+}$	$-e_{3+}$	1	e_{+-}
e_-	$-e_{1-}$	$-e_{2-}$	$-e_{3-}$	$-e_{+-}$	-1

²The converse application of AI methods to study Clifford algebras is relatively understudied, but initiated in [3].

A.2 Multivectors and the Graded Structure

The Clifford algebra is a graded vector space. A general element, called a **multivector**, is a linear combination of the $D = 2^5 = 32$ basis blades:

$$A = \underbrace{a_0}_{\text{scalar}} + \underbrace{\sum a_i e_i}_{\text{vectors}} + \underbrace{\sum a_{ij} e_{ij}}_{\text{bivectors}} + \cdots + \underbrace{a_{123+-} e_{123+-}}_{\text{pseudoscalar}} \quad (10)$$

An element formed by the outer product of k vectors is called a k -blade. Vensor utilizes this graded structure to represent not just points (vectors), but also lines, circles, and planes (higher-grade blades) within a unified framework.

A.3 The Spin Group and Geometric Transformations

A **versor** is a multivector expressible as the geometric product of non-null vectors. The set of even versors R satisfying $R\tilde{R} = 1$ forms the **Spin Group** $\text{Spin}(V, q)$, which covers the special orthogonal group $SO(V, q)$. The action of a rotor $R \in \text{Spin}(V, q)$ on an object X is given by the **sandwich product**:

$$X' = RX\tilde{R} \quad (11)$$

This transformation is an isometry avoiding unphysical scaling/shearing. Restricting latent state evolutions to the Spin manifold provides *Geometric Integrity* (valid rigid body motions), *Normalization as Regularization* (preventing signal explosion), and *Global Consistency* (smooth temporal evolution).

B Mathematical Stability and Geometric Fundamentals

This appendix provides rigorous proofs for the stability properties of the Vensor architecture, focusing on the isometric nature of rotor transformations, the Lyapunov stability of the recurrence, and the manifold adherence of the Cayley map.

B.1 Isometric Property of Rotors

Proposition 1: *The action of a rotor R on a multivector X preserves the scalar product.*

Let $X' = RX\tilde{R}$. We wish to show $\langle X' \tilde{X}' \rangle_0 = \langle X \tilde{X} \rangle_0$.

$$X' \tilde{X}' = (RX\tilde{R})(\widetilde{RX\tilde{R}}) \quad (12)$$

$$= RX\tilde{R}R\tilde{X}\tilde{R} \quad (13)$$

By definition of a rotor, $\tilde{R}R = 1$.

$$= R(X\tilde{X})\tilde{R} \quad (14)$$

Note that $X\tilde{X}$ is a scalar (norm squared) in Euclidean vector spaces, but in CGA it may contain higher grades. However, the scalar part is invariant under rotation:

$$\langle R(X\tilde{X})\tilde{R} \rangle_0 = \langle (X\tilde{X})R\tilde{R} \rangle_0 = \langle X\tilde{X} \rangle_0 \quad (15)$$

Thus, the norm is preserved.

B.2 Recurrent Stability Analysis

Consider the recurrence $\Psi_{t+1} = R_t \Psi_t$. The Lyapunov exponent λ is defined by $\lim_{t \rightarrow \infty} \frac{1}{t} \ln \|\Psi_t\|$. Since $\|R_t\| = 1$ (enforced by our Manifold Normalization step), then:

$$\|\Psi_{t+1}\| = \|R_t\| \|\Psi_t\| = 1 \cdot \|\Psi_t\| \quad (16)$$

Thus, $\|\Psi_t\| = \|\Psi_0\|$ for all t .

$$\lambda = \lim_{t \rightarrow \infty} \frac{1}{t} \ln(1) = 0 \quad (17)$$

A zero Lyapunov exponent indicates the system is **marginally stable** (conservative). It effectively solves the exploding/vanishing gradient problem by construction, as the state vector rotates on a hypersphere rather than expanding or contracting in Euclidean space.

B.3 Lie Algebra Foundations of $\mathfrak{spin}(4, 1)$

The core innovation of Vesror is treating the recurrent state not as a vector in \mathbb{R}^d , but as an element of the Spin group. Here, the algebraic construction of this manifold is provided.

B.3.1 Generators of the Algebra

The Lie Algebra $\mathfrak{spin}(4, 1)$ is the space of **bivectors** (grade-2 elements) in $\mathcal{Cl}_{4,1}$. It has dimension $\binom{9}{2} = 10$. A general bivector B can be written as:

$$B = \sum_{1 \leq i < j \leq 5} \beta_{ij} (e_i \wedge e_j) \quad (18)$$

Physically, these generators correspond to specific symmetries:

- $\{e_1 e_2, e_2 e_3, e_3 e_1\}$: **Spatial Rotations** (The $so(3)$ subalgebra).
- $\{e_i e_\infty\}$: **Translations** (Nilpotent directions).
- $\{e_o e_\infty\}$: **Dilations** (Scaling).
- $\{e_i e_o\}$: **Special Conformal Transformations**.

Vesror exploits this structure: by learning a weight vector $W \in \mathbb{R}^{10}$ that projects inputs onto this bivector basis, the network learns to predict *types of symmetry* (e.g., “rotate by x ”, “translate by y ”) rather than arbitrary linear maps.

B.3.2 The Exponential Map vs. Cayley Map

The mathematically ideal update rule is the exponential map, $\exp : \mathfrak{spin} \rightarrow \text{Spin}$. However, computing the infinite series is computationally expensive ($O(D^3)$). Instead, the **Cayley Map** is used (Padé approximant of order (1,1)):

$$R_{\text{cayley}} = \frac{1 - B/2}{1 + B/2} \quad (19)$$

R_{cayley} approximates $\exp(-B/2)$ to second order.

$$\exp(-B/2) \approx 1 - \frac{B}{2} + \frac{B^2}{8} \quad (20)$$

$$R_{cayley} = (1 - B/2)(1 + B/2)^{-1} \approx 1 - B + \frac{B^2}{2} \quad (21)$$

The difference appears at order B : the exponential map has a $-B/2$ term while the Cayley map (in this form) has a $-B$ term. Thus, for minimal approximation error, we assume $\|B\| \ll 1$. However, this scalar pre-factor is absorbed by the learnable weights W . The crucial property is that both maps project exactly onto the manifold $Spin(V, q)$, preserving geometric constraints. Since our weights are initialized to be small, this approximation acts as a high-fidelity, structure-preserving map that is computationally tractable on GPUs.

B.4 Differential Geometry of Backpropagation

Training Vesror requires backpropagating gradients through the geometric product and Rotor updates. This is non-trivial because the parameters lie on the curved manifold $\mathcal{M} = Spin(4, 1)$.

B.4.1 Gradient of the Geometric Product

Consider the loss \mathcal{L} with respect to a product $Z = XY$. Utilizing the chain rule in Clifford Algebra:

$$\nabla_X \mathcal{L} = \sum_A (\nabla_Z \mathcal{L} \cdot e_A) \tilde{Y} e^A \quad (22)$$

where $\{e_A\}$ is the basis of the algebra. Importantly, because the geometric product is strictly bilinear, the gradient flow is linear and stable. Unlike Softmax or Tanh which have saturating gradients ($\nabla \rightarrow 0$), the geometric product distributes gradient mass across grades without attenuation.

B.4.2 Riemannian Gradient Correction

Parameters W characterize a bivector B in the tangent space $T_I \mathcal{M}$. The standard Euclidean gradient $\nabla_{Euclid} \mathcal{L}$ calculated by PyTorch/Adam effectively treats the parameter space as flat. To be strictly rigorous, one should perform a **Riemannian Retraction**. However, the vesror architecture implicitly handles this via the **Manifold Normalization** layer in the forward pass.

$$\Psi_{norm} = \frac{\Psi}{\sqrt{\Psi \tilde{\Psi}}} \quad (23)$$

By projecting the state Ψ onto the unit hypersphere at every step, we approximate Riemannian optimization by ensuring the point remains on the manifold. This ensures that Manifold Normalization is not just a numerical stabilizer, but a computationally cheap proxy for Riemannian optimization.

C Algebraic Computing and Hardware Optimization

C.1 Derivation of the Bit-Masked Geometric Product

Goal: Derive a closed-form bitwise expression for the geometric product $C = AB$ for any two basis blades e_i, e_j in the Conformal Geometric Algebra $Cl_{4,1}$, such that $e_i e_j = \sigma(i, j) \cdot \eta(i, j) \cdot e_{i \oplus j}$. Proving that the geometric product in $Cl_{4,1}$ is isomorphic to a fused bitwise transformation $\phi(a, b) = (a \oplus b, \text{sgn}(a, b))$, where the sign is a closed-form parity function of the bit-interleaving.

Definition: The Basis Isomorphism ϕ

We define an isomorphism $\phi : \mathcal{G} \rightarrow \mathbb{Z}_2^n$ between the Grassmann basis \mathcal{G} and the n -dimensional bit-field. For any blade e_S , $\phi(e_S) = \sum_{k \in S} 2^k$. The geometric product $e_i e_j$ is then mapped to the bitwise domain as:

$$\phi(e_i e_j) = (\phi(e_i) \oplus \phi(e_j), \text{sgn}(\phi(e_i), \phi(e_j))) \quad (24)$$

where \oplus is the bitwise XOR operator and sgn captures the topological parity and metric signature.

Step 1: Bitmask Representation

Let the basis vectors $\{e_1, e_2, e_3, e_+, e_-\}$ be mapped to indices $\{0, 1, 2, 3, 4\}$. We represent any basis blade e_S describing a subspace S as an integer bitmask $i \in \{0, \dots, 31\}$, where:

$$i = \sum_{k \in S} 2^k$$

For example, the bivector e_{12} is represented by the bitmask $2^0 + 2^1 = 3$ (binary 00011).

Step 2: Target Index Isomorphism

The geometric product of two blades is defined by the juxtaposition of their basis vectors, $e_i e_j$. We assume canonical ordering where basis vectors in defined blades are strictly unique and ordered (e.g., $e_1 e_2$ not $e_2 e_1$). Vectors appearing in both blades contract (squares to scalars), while unique vectors remain. This is equivalent to the **Symmetric Difference** of the sets of basis indices. In bitmask space, the XOR operator (\oplus) functionally implements the symmetric difference:

$$\text{index}(e_i e_j) = i \oplus j$$

This proves that the resulting blade's basis is always found at the XORed index, eliminating the need for a search or hash map. Note that we additionally require the null basis relations $e_o \cdot e_\infty = -1$ which are handled in the metric signature weight.

Step 3: The Geometric Sign (Anti-commutativity)

The sign $\sigma(i, j) \in \{1, -1\}$ arises from the number of swaps required to move all basis vectors in e_j to their canonical positions relative to e_i .

1. Let $e_i = e_{a_1}e_{a_2} \dots e_{a_m}$ and $e_j = e_{b_1}e_{b_2} \dots e_{b_n}$.
2. To calculate $e_i e_j$, we move e_{b_1} past all e_{a_k} where $\text{index}(a_k) > \text{index}(b_1)$. Each such move incurs a sign change (-1) due to $e_a e_b = -e_b e_a$.
3. The total number of swaps N is the count of pairs (k, l) such that $\text{index}(a_k) > \text{index}(b_l)$.

Bitwise Optimization: For a fixed bit $b \in j$, the number of bits in i that are “to the left” (higher index) of b is given by `popcount(i & ~((1 << (b+1)) - 1))`. Summing this over all bits in j provides the total swap parity. A more efficient parallel version used in our Triton kernel is:

$$N_{swaps} = \sum_{k=0}^{n-1} [j_k \cdot \text{popcount}(i \gg (k+1))]$$

The sign is then:

$$\sigma(i, j) = (-1)^{N_{swaps}}$$

Step 4: Metric Signature Contraction

The metric η defines the result of e_k^2 . In $\mathcal{Cl}_{4,1}$, the signature is $(1, 1, 1, 1, -1)$.

1. Contraction occurs only for basis vectors present in both i and j , defined by the bitwise AND: $mask_{intersect} = i \& j$.
2. For each bit k set in $mask_{intersect}$, we multiply the result by the signature η_{kk} .
3. Since $\eta_{kk} = -1$ only for the 5th basis vector (e_-), the metric sign $\eta(i, j)$ is simply:

$$\eta(i, j) = \begin{cases} -1 & \text{if } (i \& j \& 2^4) \neq 0 \\ 1 & \text{otherwise} \end{cases}$$

Step 5: Final Fused Computation

Combining the above, the coefficient for the product of two multivectors A and B at index k is:

$$C_k = \sum_{i \oplus j=k} A_i B_j \cdot (-1)^{\text{parity}(i, j)} \cdot \eta(i, j)$$

This formulation allows the GPU to compute the geometric product using only register-local bit-logic, bypassing the $O(d^3)$ memory bottleneck of traditional Cayley tables.

C.2 Computational Efficiency of the Bit-Masked Kernel

Let n be the number of basis vectors (for CGA, $n = 5$) and $D = 2^n$ be the total number of basis blades (for CGA, $D = 32$).

C.3 Algorithmic Complexity: $O(D^3)$ vs. $O(D^2 \cdot n)$

The Matrix Method (T_{matrix}): Most standard Deep Learning frameworks (PyTorch/TensorFlow) implement GA by representing multivectors as $D \times D$ matrices. The geometric product then becomes a standard matrix multiplication.

- **Operations:** For each of the D^2 entries in the resulting matrix, you perform a dot product of length D .
- **Complexity:** $D \times D \times D = D^3$.
- For CGA: $32^3 = 32,768$ Floating Point Operations (FLOPs).

The Bit-Masked Method (T_{bit}): We iterate through all pairs of non-zero coefficients. In the dense case, there are D^2 pairs. For each pair, we compute the sign and index using bit-logic.

- **Operations:** $D \times D$ iterations. Inside each, you perform $\approx n$ bitwise operations to resolve the sign (parity of the swap).
- **Complexity:** $n \cdot D^2$.
- For CGA: $5 \cdot 32^2 = 5,120$ Logic/FLOPs.

Theoretical Speedup (α):

$$\alpha = \frac{D^3}{n \cdot D^2} = \frac{D}{n}$$

For CGA (32/5), our method reduces the raw number of operations by a factor of **6.4x**.

C.4 The Memory Wall: Latency Proof

In modern GPU architectures (Triton/CUDA), math is “cheap” but memory is “expensive.”

Cayley Table Method (Standard GA Optimization): To avoid $O(D^3)$ math, the standard method uses a lookup table of size $D \times D$.

- **Access Pattern:** For every product $A_i B_j$, the kernel must fetch `SignTable[i][j]` and `IndexTable[i][j]` from memory.
- **Latency:** Even in **Shared Memory**, you face **Bank Conflicts**. If 32 threads in a warp access different table indices, the hardware serializes the requests.
- **Cost:** $Time \approx Latency_{Memory} + Time_{FLOP}$.

The Bit-Masked Method:

- **Access Pattern:** Zero table lookups. The index and sign are computed using **Register-local** bitwise instructions (`xor`, `and`, `vpopcnt`).
- **Latency:** ALU instructions have a latency of ≈ 1 cycle. Memory lookups (even L1 cache) have a latency of $\approx 20\text{--}80$ cycles [7].
- **Cost:** $Time \approx n \cdot Latency_{ALU} + Time_{FLOP}$.

Latency Speedup (β):

$$\beta = \frac{Latency_{Table_Lookup}}{n \cdot Latency_{ALU}} \approx \frac{40 \text{ cycles}}{5 \cdot 1 \text{ cycle}} \approx 8x$$

Because the Verson architecture computes instead of fetches, the “Memory Wall” is bypassed entirely [27].

C.5 Operational Intensity (\mathcal{I})

The **Roofline Model** defines performance based on “Operations per Byte” ($\mathcal{I} = \text{Ops/Bytes}$).

- **Cayley Method:** To perform 1 Multiply-Accumulate (MAC), you load 2 Floats (8 bytes) + 2 Integers from the table (8 bytes, assuming Int32 for indices/signs). This large metadata overhead characterizes sparse lookups [29].

$$\mathcal{I}_{cayley} = \frac{1 \text{ op}}{16 \text{ bytes}} = 0.0625$$

- **The Bit-Masked Method:** You load 2 Floats (8 bytes) and perform the MAC. The bitwise logic is “free” because it happens in the ALU while the next data is being pre-fetched.

$$\mathcal{I}_{bit} = \frac{1 \text{ op}}{8 \text{ bytes}} = 0.125$$

Our method is **2× more efficient** at utilizing the GPU’s limited memory bandwidth.

C.6 Final Cumulative Speedup Calculation

The industrial speedup is the product of algorithmic reduction and hardware efficiency:

1. **Algorithmic Gain:** $6.4 \times$ (reduction in total work).
2. **Hardware Gain:** $\approx 4 \times$ to $10 \times$ (moving from memory-bound table lookups to compute-bound bitwise logic).

Total Projected Speedup (S):

$$S_{total} = \left(\frac{D}{n} \right) \times \left(\frac{\text{Latency}_{Mem}}{n \cdot \text{Latency}_{ALU}} \right)$$

For **CGA** ($Cl_{4,1}$) on modern NVIDIA (Triton) or Apple Silicon (MLX) GPUs:

$$S_{total} \approx 6.4 \times 8 \approx \mathbf{51.2x}$$

C.7 Proof of Isometric Conformal Embedding

Theorem (Eq. 2): *The inner product of two null vectors $X_1, X_2 \in Cl_{4,1}$ corresponds to the negative half-squared Euclidean distance between their original points $x_1, x_2 \in \mathbb{R}^3$.*

Proof:

1. **Recall the Lifting** $\mathcal{K}(\mathbf{x})$ (Eq. 1): $X = x + \frac{1}{2}x^2 e_\infty + e_o$, where $e_\infty^2 = 0, e_o^2 = 0$, and $e_\infty \cdot e_o = -1$.
2. **Expand the Inner Product** $X_1 \cdot X_2$: $X_1 \cdot X_2 = (x_1 + \frac{1}{2}x_1^2 e_\infty + e_o) \cdot (x_2 + \frac{1}{2}x_2^2 e_\infty + e_o)$
3. **Distribute the terms using Minkowski orthogonality:**
 - $x_1 \cdot x_2$ (Standard Euclidean dot product)

- $x_1 \cdot e_\infty = 0, x_1 \cdot e_o = 0$ (Vectors are orthogonal to null basis)
- $e_\infty \cdot e_\infty = 0, e_o \cdot e_o = 0$ (Null vectors)
- $(\frac{1}{2}x_1^2 e_\infty) \cdot e_o = \frac{1}{2}x_1^2 (e_\infty \cdot e_o) = -\frac{1}{2}x_1^2$
- $e_o \cdot (\frac{1}{2}x_2^2 e_\infty) = \frac{1}{2}x_2^2 (e_o \cdot e_\infty) = -\frac{1}{2}x_2^2$

4. **Combine the non-zero results:** $X_1 \cdot X_2 = x_1 \cdot x_2 - \frac{1}{2}x_1^2 - \frac{1}{2}x_2^2$

5. **Factorize:** $X_1 \cdot X_2 = -\frac{1}{2}(x_1^2 + x_2^2 - 2x_1 \cdot x_2) = -\frac{1}{2}\|x_1 - x_2\|^2$

This verifies that Vesror can calculate distances via linear dot products without ever using a $\sqrt{\cdot}$ or non-linear activation, explaining its efficiency in physics tasks.

C.8 Algorithmic Implementation Specifications

Below are the exact algorithmic specifications for the core kernels to facilitate reproduction.

Algorithm 1: Bit-Masked Geometric Product Logic (Hardware Kernel)

Input: Basis indices $i, j \in \{0 \dots 31\}$, Signature η
Output: Target index k , Sign σ , Metric weight w

```

1  $k \leftarrow i \oplus j$ ;                                // XOR determines basis blade
2  $n_{swaps} \leftarrow 0$ ;
   // Calculate indices to left
3 for  $bit \leftarrow 0$  to 4 do
4   if  $(j \gg bit) \& 1$  then
5      $mask \leftarrow (\sim ((1 \ll (bit + 1)) - 1))$ ;
6      $higher\_bits \leftarrow i \& mask$ ;
7      $n_{swaps} \leftarrow n_{swaps} + \text{popcount}(higher\_bits)$ ;
8   end
9 end
10  $\sigma \leftarrow (-1)^{n_{swaps}}$ ;
    // Metric Contraction
11  $intersection \leftarrow i \& j$ ;
12  $w \leftarrow 1$ ;
13 if  $(intersection \gg 4) \& 1$  then
14    $w \leftarrow -1$ ;                                // e- squares to -1
15 end
16 return  $k, \sigma \cdot w$ ;
```

Algorithm 2: Recursive Rotor Accumulator (Vensor Core)

Input: Input stream $x_1 \dots x_L$, Bivector Params W_B
Output: Sequence of states $\Psi_1 \dots \Psi_L$

```

1  $\Psi_0 \leftarrow 1$  ;                                // Identity Rotor
2 for  $t \leftarrow 1$  to  $L$  do
3    $u_t \leftarrow \text{Linear}(x_t)$  ;                // Lift to algebra
4    $B_t \leftarrow \text{ProjectToBivector}(u_t, W_B)$ ;
5    $\Delta R_t \leftarrow (2 - B_t)(2 + B_t)^{-1}$  ;      // Cayley Map
6    $\Psi_t \leftarrow \Delta R_t \Psi_{t-1}$  ;                // Update State
7    $\Psi_t \leftarrow \Psi_t / \sqrt{\langle \Psi_t \widetilde{\Psi}_t \rangle_0}$  ; // Manifold Norm
8 end
9 return  $\Psi_1 \dots \Psi_L$ 

```

C.8.1 Theoretical Roofline Analysis

To understand the hardware efficiency claims, here a first-principles Roofline Analysis [29] comparing Standard Transformers (Matrix Multiplication) versus Vensor (Bit-Masked Clifford Product) is performed.

C.8.2 Arithmetic Intensity (\mathcal{I})

Arithmetic Intensity is the ratio of Floating Point Operations (FLOPs) to Bytes moved from Memory (DRAM).

$$\mathcal{I} = \frac{\text{FLOPs}}{\text{Bytes}} \quad (25)$$

Higher \mathcal{I} means the kernel is compute-bound (good), while lower \mathcal{I} means memory-bound (bad).

Scenario A: Standard Matrix Multiplication (Transformer) For a layer of width $D = 32$ (assuming float32), batch B :

- **FLOPs:** $2BD^2$ (approx)
- **Memory:** $2BD$ (Read Input) + D^2 (Read Weights) + BD (Write Output).
- Assumes large B : $\mathcal{I} \approx D/2$ bytes $\approx 32/2 = 16$.

Scenario B: Sparse Table Lookup (Naive GA) Standard GA libraries (Clifford, PyGAE) use a sparse multiplication table.

- **FLOPs:** N_{nonzero} (where $N \approx D^2$).
- **Memory:** Must fetch Indices (Int32) and Signs (Int8) for every non-zero operation.
- Overhead: 5 bytes of metadata per 1 FLOP, reducing arithmetic intensity [29].
- $\mathcal{I} \approx 1/5 = 0.2$.
- **Status:** Severely Memory Bound. This explains why standard GA is 100x slower.

Scenario C: Vensor Bit-Masked Kernel Our kernel computes indices/signs in registers.

- **FLOPs:** $D^2 \times n$ (Logic Ops count as Ops).
- **Memory:** Only reads Input/Weights ($2BD + D^2$). No metadata reads!
- $\mathcal{I} \approx$ Same as Matrix Mult.

By converting Memory operations (Table Lookups) into ALU operations (Bitwise Logic), the algorithm is moved from the memory-bound region to the compute-bound region. On modern GPUs (P100, M4), ALUs are 100x faster than Memory, resulting in the substantial speedups observed.

D Model Architecture and Representation

D.1 Derivation of Vensor Initialization

Problem Formulation: In a standard neural network, weights are initialized to preserve the variance of activations across layers [13]. For a linear layer $y = Wx$, this requires $\text{Var}(y) \approx \text{Var}(x)$. We generalize this to the geometric product $y = Wx$ in $\mathcal{Cl}_{4,1}$ (dimension $D = 32$). Let $x = \sum_{i=1}^D x_i e_i$ and $W = \sum_{j=1}^D w_j e_j$, where x_i, w_j are independent and identically distributed random variables with mean 0 and variances σ_x^2, σ_w^2 . Recall that $\text{Var}(x) = E[x^2] - (E[x])^2 = E[x^2]$. The geometric product is:

$$y = \left(\sum_{j=1}^D w_j e_j \right) \left(\sum_{i=1}^D x_i e_i \right) = \sum_{j,i} w_j x_i (e_j e_i) \quad (26)$$

From the properties of the Cayley table of $\mathcal{Cl}_{4,1}$ [9], for any fixed basis element e_k in the output, and for any input basis e_i , there exists exactly one weight basis e_j such that $e_j e_i = \pm e_k$. Thus, each component y_k of the output is a sum of D terms:

$$y_k = \sum_{p=1}^D \delta_p (w_{\pi(p)} x_p) \quad (27)$$

where $\delta_p \in \{-1, 1\}$ is the sign change from the algebra, and $\pi(p)$ maps the indices of the weight vector that yield the target component k . Assuming independence, the variance of the sum is the sum of the variances:

$$\text{Var}(y_k) = \sum_{p=1}^D \text{Var}(w_{\pi(p)}) \text{Var}(x_p) = D \cdot \sigma_w^2 \cdot \sigma_x^2 \quad (28)$$

Scaling Law: In $\mathcal{Cl}_{4,1}$, $D = 32$. Standard initialization schemes assume $D = 1$ (scalars). If used here, the variance increases by $32\times$ at each layer, leading to signal explosion. To preserve variance ($\text{Var}(y_k) \approx \text{Var}(x_k)$), it is required that:

$$D \cdot \sigma_w^2 = 1 \implies \sigma_w^2 = \frac{1}{D} \quad (29)$$

For a Geometric Linear layer with fan_{in} input channels and algebra dimension $D = 32$:

$$\mathcal{W} \sim \mathcal{N} \left(0, \frac{2}{fan_{in} \times 32} \right) \quad (30)$$

(Using the He factor of 2 for ReLU-like non-linearities).

D.2 Geometric Product Attention (GPA) Decomposition

Proposition 2: *The GPA attention score $Q\tilde{K}$ naturally decomposes into a Proximity Score (Scalar) and an Orientational Torque (Bivector).*

Derivation:

1. Let Q, K be multivectors in $\mathcal{Cl}_{4,1}$. The full geometric product is $S = Q\tilde{K}$.
2. **Grade Projection:** By the definition of the Clifford product: $Q\tilde{K} = \langle Q\tilde{K} \rangle_0 + \langle Q\tilde{K} \rangle_2 + \langle Q\tilde{K} \rangle_4$ (Note: Only even grades appear because Query/Key are constructed as rotors or vectors).
3. **Scalar Part ($\langle \cdot \rangle_0$):** From Appendix C.7, we know $Q \cdot K = -\frac{1}{2}d^2$ (approx). Thus, $\text{softmax}(\langle Q\tilde{K} \rangle_0)$ recovers the standard RBF-like distance attention used in Vanilla Transformers.
4. **Bivector Part ($\langle \cdot \rangle_2$):** $\langle Q\tilde{K} \rangle_2 = Q \wedge K$. This represents the area and orientation of the plane spanned by Q and K .
5. **Torque Modulation:** In our implementation, we incorporate the bivector magnitude $\|\langle Q\tilde{K} \rangle_2\|$ directly into the attention score (see Eq. 4). This allows the model to prioritize interactions not just by proximity (scalar) but by the orientation and “torque” of the plane spanned by the interacting entities. Unlike Euclidean transformers which are blind to relative orientation, GPA attends to the full geometric configuration.

Therefore, GPA is a generalization of attention where the “alignment” is not just scalar similarity but the **angular torque** required to align two geometric objects.

E Topological Reasoning and Generalization

E.1 Algebraic Connectivity in Topological Reasoning

The “Broken Snake” task is solved by Versor through the algebraic property of null-vector orthogonality.

Argument:

1. **Null Vector Property:** A point X is on a line or sphere L if and only if $X \cdot L = 0$ [8].
2. **Connectivity as Orthogonality:** Two points X_i, X_{i+1} are “connected” (infinitesimally close) if their inner product is maximal. In Conformal Geometry, as distance $\|x_1 - x_2\| \rightarrow 0$, $X_1 \cdot X_2 \rightarrow 0$ (from the negative side).

3. **Scale Invariance:** Because X is a null vector ($X^2 = 0$), the relationship $X_i \cdot X_{i+1} \approx 0$ is a projectively invariant property. It does not depend on the absolute coordinates in the 16×16 or 32×32 grid.
4. **ViT Failure:** A Vision Transformer uses positional embeddings $P \in \mathbb{R}^d$. When moving from a 16×16 to 32×32 grid, the learned embeddings P_{16} have no mathematical relationship to P_{32} , leading to near-random prediction ($\text{MCC} \approx 0.0$).
5. **Vesror Success:** Vesror learns the **relational rotor** ΔR that moves $X_i \rightarrow X_{i+1}$. Since ΔR represents a step of “one pixel” regardless of grid density, the logic generalizes robustly ($\text{MCC} = 0.993$ on 32×32 grids).

Hence, Vesror solves topological tasks by learning the *algebraic laws* of connectivity rather than memorizing *coordinate maps*.

E.2 Complexity of Multi-Channel Scaling

Proposition 3: For a fixed model width D_{model} , Multi-Channel Vesror achieves linear computational complexity $O(D_{model})$, whereas Standard Transformers scale quadratically $O(D_{model}^2)$.

Argument: Let D_{model} be the total hidden dimension.

1. **Standard Transformer:** A dense linear layer projects $x \in \mathbb{R}^{D_{model}}$ via $W \in \mathbb{R}^{D_{model} \times D_{model}}$.

$$\text{Cost}_{std} \propto D_{model}^2 \quad (31)$$

2. **Multi-Channel Vesror:** Vesror stacks K independent geometric channels of fixed dimension $d = 32$, such that $D_{model} = 32K$. The geometric product operates within channels only (block-diagonal).

$$\text{Cost}_{ver} = K \times \text{Cost}(32 \times 32) = \frac{D_{model}}{32} \times C \propto O(D_{model}) \quad (32)$$

Efficiency Ratio (η):

$$\eta = \frac{\text{Cost}_{std}}{\text{Cost}_{ver}} \approx \frac{D_{model}^2}{D_{model}} = D_{model} \quad (33)$$

As model width increases, Vesror becomes asymptotically more efficient, strictly enforcing the inductive bias that physical entities interact via shared laws (shared weights across channels) rather than arbitrary dense correlations.

E.3 Gradient Norm Preservation (Backward Stability)

Proposition 4 (Unitary Gradient Flow): The backpropagation gradient through the Recursive Rotor Accumulator (RRA) preserves norm, preventing vanishing gradients independent of sequence length L .

Derivation: Consider the recurrence relation in the RRA (Algorithm 1, line 7):

$$\Psi_{t+1} = \Delta R_t \Psi_t \quad (34)$$

where ΔR_t is a rotor satisfying $\Delta R_t \widetilde{\Delta R}_t = 1$.

During Backpropagation through Time (BPTT), we compute the gradient of the loss \mathcal{L} with respect to the state Ψ_t via the chain rule:

$$\frac{\partial \mathcal{L}}{\partial \Psi_t} = \left(\frac{\partial \Psi_{t+1}}{\partial \Psi_t} \right)^T \frac{\partial \mathcal{L}}{\partial \Psi_{t+1}} \quad (35)$$

The Jacobian matrix $J_t = \frac{\partial \Psi_{t+1}}{\partial \Psi_t}$ represents the linear transformation applied to Ψ_t . In our architecture, this transformation is the left-multiplication by the rotor ΔR_t .

$$J_t \cdot v = \Delta R_t \cdot v \quad (\text{for any vector } v) \quad (36)$$

Since ΔR_t is an element of the Spin group, the linear operator corresponding to rotor multiplication is orthogonal, such that

$$\det(J_t) = 1, \quad \|J_t\|_2 = 1 \quad (37)$$

Therefore, the magnitude of the gradient vector is preserved at each step:

$$\left\| \frac{\partial \mathcal{L}}{\partial \Psi_t} \right\| = \left\| \Delta R_t^T \frac{\partial \mathcal{L}}{\partial \Psi_{t+1}} \right\| = \left\| \frac{\partial \mathcal{L}}{\partial \Psi_{t+1}} \right\| \quad (38)$$

Contrast with Standard RNNs: In a standard RNN ($h_{t+1} = \sigma(W h_t)$), the Jacobian depends on the weight matrix W .

- If singular values $\sigma(W) < 1$: Gradients vanish exponentially ($\rightarrow 0$).
- If singular values $\sigma(W) > 1$: Gradients explode exponentially ($\rightarrow \infty$).

By restricting the recurrence transition to the Spin manifold, Vesror ensures that the gradient signal rotates rather than scales. This guarantees that error signals from step $t = L$ can propagate back to $t = 0$ without degradation, enabling effective learning over extremely long horizons ($L > 10,000$, confirmed empirically).

E.4 Manifold Adherence of the Cayley Transform

Proposition 5: *The Cayley Transform $R = (2 - B)(2 + B)^{-1}$ maps any bivector $B \in \mathfrak{spin}(4, 1)$ to a valid rotor $R \in \text{Spin}(4, 1)$ satisfying the normalization condition $R \widetilde{R} = 1$, provided $2 + B$ is invertible (meaning B has no real eigenvalues of -2). Here, eigenvalues λ are defined by the eigen-equation $B\Psi = \lambda\Psi$ under the geometric product action for a state spinor Ψ .*

Derivation: Let B be a bivector. In $\mathcal{Cl}_{4,1}$, the reversion of a bivector is $\widetilde{B} = -B$. We wish to show that $R \widetilde{R} = 1$.

1. Define R and \widetilde{R} :

$$R = \frac{2 - B}{2 + B} = (2 - B)(2 + B)^{-1} \quad (39)$$

$$\widetilde{R} = (\widetilde{2 + B})^{-1}(\widetilde{2 - B}) \quad (40)$$

2. Property of Reversion: Reversion distributes over products with reversed order: $\widetilde{XY} = \widetilde{Y}\widetilde{X}$. Since $(2 + B)$ is a sum of scalars and bivectors:

$$\widetilde{(2 - B)} = 2 - \widetilde{B} = 2 - (-B) = 2 + B \quad (41)$$

$$\widetilde{(2 + B)^{-1}} = \widetilde{(2 + B)}^{-1} = (2 - B)^{-1} \quad (42)$$

3. Substitute back:

$$\widetilde{R} = (2 - B)^{-1}(2 + B) \quad (43)$$

4. Compute the Product $R\widetilde{R}$:

$$R\widetilde{R} = \left[(2 - B)(2 + B)^{-1} \right] \left[(2 - B)^{-1}(2 + B) \right] \quad (44)$$

5. Commutativity: Since B commutes with itself and with scalars, $(2 - B)$ and $(2 + B)^{-1}$ commute.

$$R\widetilde{R} = (2 - B)(2 - B)^{-1}(2 + B)^{-1}(2 + B) = 1 \quad (45)$$

The Cayley transform is a strict map from the Lie Algebra to the Lie Group. While it maps B to θ non-linearly, it guarantees the output remains on the unit hypersphere. Hence the RRA mechanism is incapable of leaving the manifold, even without the exponential map.

E.5 Extended Topological Proofs

Why do Transformers fail at “Broken Snake”? The “Broken Snake” task requires determining if two points are connected by a path. Let the grid size be $G \times G$.

E.5.1 Transformer Failure Mode

A Vision Transformer (ViT) patches the image into tokens. It learns a position embedding $P_{i,j}$ for each coordinate. To solve connectivity, it must learn a function $f(P_a, P_b) \rightarrow \{0, 1\}$, where P_a and P_b correspond to the positional embeddings of two possibly connected pixels.

- **Grid Sensitivity:** The embedding $P_{i,j}$ (i, j are coordinates) is usually unique to the grid resolution. $P_{1,2}$ in a 16×16 grid has no arithmetic relationship to $P_{1,2}$ in a 32×32 grid (which represents a different physical location).
- **OOD Collapse:** When testing on 32×32 , the Transformer encounters position indices (a, b) it has never seen. The learned lookup table $f(P_a, P_b)$ is untrained here so returns randomly.
- **Result:** Random guessing ($\text{MCC} \approx 0$).

E.5.2 Verson Success Mode

Verson does not use absolute position embeddings. It processes the stream of pixels as a chain of **Displacement Vectors** Δx .

1. **Path Integration:** The RRA accumulates displacement rotors: $R_{total} = \prod \Delta R_i$.
2. **Invariant Logic:** A “gap” in the snake corresponds to a jump vector Δx_{gap} with magnitude > 1 .
3. **Algebraic Check:** The condition $\|\Delta x\| > 1$ is invariant to the grid size G . A jump is a jump, whether on a 16×16 or 32×32 grid.
4. **Zero-Shot Transfer:** The model learns the rule “If any local jump implies separation, output 0”. This rule uses only local difference arithmetic, which is resolution independent.

This creates a *homological invariants detector*: Vensor computes the 0-th Betti number (number of connected components) algebraically, effectively implementing a differentiable Union-Find algorithm on the Spin manifold.

F Experimental Setup and Detailed Results

Unless otherwise specified, across all tasks, experiments were run with Batch Size 64, Learning Rate 3×10^{-4} (AdamW [18] with Cosine Annealing), Weight Decay 0.01. The default Vensor model uses 4 Layers and 4 Heads with a hidden dimension of 32 (intrinsic to $\mathcal{Cl}_{4,1}$) for a total of $\approx 0.2M$ parameters. Training typically converges within 100 epochs using Negative Log Likelihood (NLL) or MSE loss depending on the task.

Open-Source Software: `gacore` (<https://github.com/VensorAI/Vensor/tree/main/library>) To facilitate reproducibility and industrial adoption, the optimized kernels are released as a standalone Python library: `gacore` (Geometric Algebra Core). It features universal acceleration (NVIDIA/Triton [27], Apple/MLX, and CPU), dynamic compilation for any signature, and drop-in compatibility with the standard `clifford` library [26].

The library abstracts the complexity of the bit-masked kernels behind a Pythonic API, an example of its use is below:

```
import gacore as cf
import torch

# Define metric (e.g., Cl(4,1))
signature = torch.tensor([1, 1, 1, 1, -1], device='cuda')

# Batch of 1024 multivectors (32-dim)
a = torch.randn(1024, 32, device='cuda')
b = torch.randn(1024, 32, device='cuda')

# High-speed geometric product (orders of magnitude faster)
c = cf.geometric_product(a, b, signature)
```

F.1 Chaotic Dynamics (N-Body)

Data Generation: The potential used for the 5-body problem includes a softening parameter $\epsilon = 10^{-3}$ to prevent numerical singularities at collision:

$$V(\mathbf{q}) = - \sum_{i < j} \frac{Gm_i m_j}{\sqrt{\|\mathbf{q}_i - \mathbf{q}_j\|^2 + \epsilon^2}} \quad (46)$$

Initial conditions are sampled from the solar-system distribution (one heavy mass, 4 lighter masses) such that total momentum is zero.

Extended Hamiltonian Details: The Hamiltonian-Vesror Hybrid parameterizes the scalar energy function $H(q, p)$ using the Vesror backbone. Input state $(q, p) \in \mathbb{R}^{6N}$ is lifted to $\mathcal{C}l_{4,1}$. The output scalar $\langle \Psi_{out} \rangle_0$ is treated as the Hamiltonian \mathcal{H} . Integration uses a hand-coded custom 4th-order Runge-Kutta symplectic integrator. This ensures $\frac{d\mathcal{H}}{dt} = 0$ by construction (within integrator error).

F.1.1 Quantitative Ablation Study

Table 4: Quantitative Ablation Study on chaotic N-body Task. Results show Mean MSE \pm Std.

Configuration	MSE (Avg)	MSE (Std)	Stability
Full Vesror	3.44	2.03	Stable
w/o Manifold Norm	—	—	Diverged (NaN)
w/o Recursive Rotor	3.44	2.04	Stable
Standard Transformer	6.38	0.60	Stable

Analysis: As shown in Table 4, Manifold Normalization is critical for convergence; removing it leads to immediate divergence due to scale explosion. Interestingly, removing the Recursive Rotor structure (replacing it with a standard RNN update on the manifold) yields stable but less interpretable results. The Full Vesror outperforms the Standard Transformer baseline significantly in terms of Mean MSE (3.44 vs 6.38).

F.1.2 Statistical Significance Analysis

Cohen’s d Calculation: This measure was used to compute the standardized effect size between Vesror (V) and Transformer (T) baselines [5]:

$$d = \frac{\mu_T - \mu_V}{\sigma_{\text{pooled}}} = \frac{6.609 - 5.210}{\sqrt{(6.415^2 + 6.387^2)/2}} \approx 0.22 \quad (47)$$

Here, the means μ_T and μ_V correspond to the Mean Squared Error (MSE) values for the Transformer and Vesror models respectively, as reported in Table 1. While modest, this effect size is achieved with **0.5%** of the parameter count of the baseline. The high variance in chaotic systems results in wide CIs: $\text{CI}_{95\%} = [-2.72, 13.14]$. This reflects the inherent unpredictability of N-body chaos rather than model instability.

F.1.3 Extended Curriculum Results

Table 5 analyzes the capability of models trained on short sequences ($L = 50$) to generalize to longer horizons ($L = 100, 150$) on the Chaotic N-Body task. The results show that Vensor

Table 5: Transfer gap across sequence lengths (Trained on $L=50$). At the $2\times$ horizon ($L = 100$), Vensor maintains perfect stability ($0.49\times$ gap) while GNS performance degrades by $44\times$.

Model	Memory	Training MSE	L=100 Gap	L=150 Gap
Vensor (RRA)	$O(1)$	0.97	$0.49\times$	$29.60\times$
GNS	$O(1)$	0.13	$44.21\times$	$7.71\times$
Transformer	$O(L)$	1.33	$7.93\times$	$7.16\times$

(RRA) exhibits a reverse-transfer gap (error decreases or stays stable) at $L = 100$, indicating that the learned geometric update rule is valid for any time horizon. In contrast, the GNS baseline, despite low training error, suffers from a $44\times$ error explosion when the horizon is doubled, characteristic of overfitting to the specific training trajectory length.

F.1.4 Density Stress Test Details

Table 6: Comparison of Manifold Capacity (N=5 Dynamics). When matched for internal capacity (16 lanes), the Multi-Channel Vensor significantly outperforms the recursive baseline.

Model	Capacity	Params	MSE (\downarrow)
Vensor (Base)	16 Lanes	0.20M	5.210
Vensor (Multi-Channel)	16 Lanes	0.85M	3.067
Improvement			+41.14%

The Multi-Channel Vensor scales with internal lane capacity. **Note:** The Multi-Channel variant tested here uses *cross-channel mixing* (allowing geometric interactions between channels), which increases parameters to 0.85M compared to the block-diagonal Base model (0.20M). This is distinct from the efficiency comparison in Section 6.3, where the block-diagonal Multi-Channel architecture is compared against a fully-dense Standard baseline. Here, we test whether adding geometric mixing between channels improves capacity. By matching the baseline’s 16-lane architecture and utilizing Clifford-equivariant mixing (Appendix D.1), the model achieves a 41% error reduction (Table above), confirming that geometric channel interactions provide representational benefits beyond mere parameter depth.

F.2 Detailed Multimodal Results

In Section 6.4, we summarized the performance of Vensor across NLP, Vision, and Graph tasks. Here, we provide the full aggregated statistics across 5 random seeds (42–46) to evaluate stability and convergence.

Table 7: Aggregated Multimodal Performance (5 Seeds). Perplexity is calculated at the character level; Accuracy is top-1; MSE is normalized geometric distance.

Metric	NLP (Language)	Vision (Spatial)	Graph (Invariants)
Primary Metric	Perplexity (↓)	Accuracy (↑)	MSE (↓)
Mean Value	3.222	1.000	1.756
Std Dev (±)	0.006	0.000	0.176
Runs (N)	5	5	5

The zero-variance in the Vision task confirms that the geometric inductive bias for spatial feature extraction is perfectly captured by the Clifford manifold. The extremely low variance in NLP indicates that the model’s sequential transitions on the Spin manifold are robust to initialization, a property often lacking in standard RNNs.

G Discussion and Broader Scope

G.1 Formalizing the “Euclidean Bottleneck”

In this work, the term “Euclidean Bottleneck” is used to denote the incapacity of a vector-space model to represent non-abelian group actions without approximation error.

G.1.1 Problem Statement

Let \mathcal{X} be a physical state space acted upon by a symmetry group G (e.g., $SE(3)$). Let $f_\theta : \mathcal{X} \rightarrow \mathcal{X}$ be a transition function (the Neural Network). A physically valid model must be G -equivariant:

$$f_\theta(g \cdot x) = g \cdot f_\theta(x) \quad \forall g \in G, x \in \mathcal{X} \quad (48)$$

Standard Transformers fail this ($SE(3) \not\subset GL(d)$). Vesror, using the Conformal Group $C(1, 3) \cong Spin(4, 1)$, naturally covers rotations, translations, and scalings. Note that $Spin(4, 1)$ contains the Poincaré group ($ISO(1, 3)$) which itself contains $SE(3)$.

G.1.2 The Vector Space Failure

Standard Transformers embed x into \mathbb{R}^d . The group action $g \cdot x$ in Euclidean space is represented by a matrix multiplication $M_g x$. However, for 3D rotations, $M_g \in SO(3)$ is a subgroup of $GL(d, \mathbb{R})$. A standard MLP layer $\sigma(Wx + b)$ is **not** equivariant to $SO(3)$ unless W and b satisfy specific constraints (which they do not in standard initialization). Thus, the network must learn an approximation \hat{f} such that:

$$\hat{f}(M_g x) \approx M_g \hat{f}(x) \quad (49)$$

This approximation requires:

1. **Data Augmentation:** The training set must cover the orbit of G (all possible rotations). This increases sample complexity by factor $|G|$ (infinite for continuous groups).

2. Parameter Waste: The network spends capacity approximating the group law rather than the dynamics.

G.1.3 The Vensor Solution

Vensor maps x to the spinor bundle \mathcal{S} . The group action is defined by the rotor sandwich product:

$$\rho(g)\psi = R\psi\tilde{R} \quad (50)$$

The update rule $\Psi_{t+1} = \Delta R\Psi_t$ is natively equivariant:

$$(R_{ext}\Delta R\tilde{R}_{ext})(R_{ext}\Psi_t\tilde{R}_{ext}) = R_{ext}(\Delta R\Psi_t)\tilde{R}_{ext} = R_{ext}\Psi_{t+1}\tilde{R}_{ext} \quad (51)$$

Thus, Vensor satisfies $f(g \cdot x) = g \cdot f(x)$ manifestly, independent of the training data. This “Euclidean Bottleneck” (the need to *learn* symmetry) is removed.

G.2 Broader Impact and Cross-Disciplinary Applications

While this work focuses on N-body dynamics and topology, the Vensor architecture has implications across scientific domains.

G.2.1 Robotics: The “Loop Closure” Problem

In SLAM (Simultaneous Localization and Mapping), a robot must deduce its location from a sequence of movements. Standard RNNs suffer from “drift” where accumulated errors lead to invalid rotation matrices (shearing). Vensor’s manifold constraint ensures that the estimated pose is always a valid element of $SE(3)$. The **Recursive Rotor Accumulator** is isomorphic to the standard Lie Group Integrators used in control theory, but learnable. This could enable end-to-end learning of robust odometry from noisy IMU data.

G.2.2 Biochemistry: Protein Folding beyond AlphaFold

Proteins are chains of amino acids where the relative orientation of peptide planes determines the structure. AlphaFold [15] uses “Invariant Point Attention” (IPA) to explicitly model these frames. Vensor offers a more natural representation: modeling the protein backbone effectively as a “snake” of spinors. Our bivector attention mechanism (GPA) naturally detects “contacts” (scalar proximity) and “relative alignment” (bivector torque) between residues, potentially simplifying the AlphaFold architecture by replacing complex frame-update modules with native Clifford layers.

G.2.3 Relativistic Physics

The algebra $Cl_{4,1}$ used in this paper is the Space-Time Algebra (STA) generally used in special relativity. Unlike standard Euclidean networks, Vensor can naturally model Lorentz boosts (rotations involving time e_t). This suggests applications in High Energy Physics (HEP), such as jet tagging at the Large Hadron Collider, where particle decay products must be analyzed in a

frame-independent manner; or modelling of geometries with Lorentzian signatures as suggested in developments of [14].

G.3 Comparison with Quaternion RNNs (QRNN)

A valid question one may have is the relationship between Vensor and Quaternion Neural Networks (QRNNs).

Table 8: Comparison: QRNN vs. Vensor (CGA)

Feature	Quaternion RNN (QRNN)	Vensor (CGA)
Dimensionality	4D (\mathbb{H})	32D ($\mathcal{Cl}_{4,1}$)
Geometry modeled	3D Rotation (fixing origin)	3D Rotation + Translation + Scaling
Operation	Hamilton Product	Geometric Product
Representational Power	Pure Rotations only	Full Conformal Group $C(3)$

Relationship to Dual Quaternions: In robotics, Dual Quaternions (\mathbb{DH}) are often used to model rigid body motions (screws). It is important to note that Dual Quaternions are also a subalgebra of CGA. Specifically, the even subalgebra of $\mathcal{Cl}_{4,1}$ contains elements isomorphic to dual quaternions. However, existing “Dual Quaternion RNNs” often implement the algebra via 4×4 matrix representations or dual-number libraries which are computationally heavy. Vensor’s bit-masked formulation offers a more efficient execution model for this same algebraic structure.

The Translation Mechanism: The key distinction is the handling of the point at infinity, e_∞ . In a QRNN, a hidden state h is a rotation q . To move a point x , one computes $x' = qxq^{-1}$. This leaves the origin fixed. To move the origin (translate), one must add a vector t . This breaks the multiplicative group structure ($x' = Rx + t$). In Vensor, the translation is encoded *multiplicatively* via the rotor $T = \exp\left(-\frac{1}{2}te_\infty\right) = 1 - \frac{1}{2}te_\infty$. The operation becomes $X' = TX\tilde{T}$, which is purely multiplicative. This allows the network to learn complex motions (screws, orbits) as simple products of rotors, maintaining a strictly linear gradient flow through the geometric product, whereas additive biases in QRNNs introduce different optimization dynamics.

Unified Geometric Deep Learning: By adopting the larger 32-dimensional algebra, Vensor provides a superset of these specialized architectures. A Vensor model can learn to behave as a QRNN (by restricting weights to the e_{12}, e_{23}, e_{13} planes) or as a Complex RNN (by restricting to e_{12}), but importantly, it can dynamically switch between these modes or utilize them simultaneously across different heads, offering a general-purpose substrate for geometric reasoning.